resources

MDPI

Article

Changes in Terrestrial Evaporation across Poland over the Past Four Decades Dominated by Increases in Summer Months

Urszula Somorowska

Department of Hydrology, Faculty of Geography and Regional Studies, University of Warsaw, Krakowskie Przedmieście 30, 00-927 Warsaw, Poland; usomorow@uw.edu.pl

Abstract: Given the importance of terrestrial evaporation (ET) for the water cycle, a fundamental understanding of the water quantity involved in this process is required. As recent observations reveal a widespread ET intensification across the world, it is important to evaluate regional ET variability. The specific objectives of this study are the following: (1) to assess annual and monthly ET trends across Poland, and (2) to reveal seasons and regions with significant ET changes. This study uses the ET estimates acquired from the Global Land Evaporation Amsterdam Model (GLEAM) dataset allowing for multi-year analysis (1980–2020). The Mann–Kendall test and the Sen's slope were applied to estimate the significance and magnitude of the trends. The results show that a rising temperature, along with small precipitation increase, led to the accelerated ET of 1.36 mm/y. This was revealed by increased transpiration and interception loss not compensated by a decrease in bare soil evaporation and sublimation. The wide-spread higher water consumption especially occurred during the summer months of June, July, and August. Comparing the two subperiods of 1980–2020, it was found that in 2007–2020, the annual ET increased by 7% compared to the reference period of 1980–2006. These results can serve as an important reference for formulating a water resources management strategy in Poland.

Keywords: terrestrial evaporation; components; Global Land Evaporation Amsterdam Model (GLEAM); increasing trends; spatial–temporal pattern; evaporative ratio; Poland

Citation: Somorowska, U. Changes in Terrestrial Evaporation across Poland over the Past Four Decades Dominated by Increases in Summer Months. *Resources* **2022**, *11*, 6. https://doi.org/10.3390/resources11010006

Academic Editor: Diego Copetti

Received: 7 December 2021
Accepted: 9 January 2022
Published: 12 January 2022

1. Introduction

Terrestrial evaporation (ET), alternatively called land surface evaporation or evapotranspiration [1], is an important component of the global water cycle. It consists of biophysical (transpiration from vegetation) and physical (evaporation from the interception, bare soil, and open water) water fluxes. The contribution of these different fluxes to the total amount of evaporated water depends on both the climate controlling the atmospheric water demand, and the land surface features, especially vegetation characteristics, influencing the energy balance at the land surface and determining the volume of interception [2]. At a global scale, the largest share in terrestrial evaporation is transpiration (Et; 59%), followed by vegetation and floor interception (Ei; 31%), soil moisture evaporation (Es; 6%), and, lastly, open water evaporation (Ew; 4%) [3]. As changes in terrestrial evaporation can lead to either warming or cooling of the land surface [4], acquiring a better understanding of ET changes is of high priority for ongoing research. Additionally, knowledge of the temporal changes of ET is necessary for accurately quantifying global and regional water budgets and for a better understanding of the hydrological interactions between the land and the atmosphere [5]. Revealing the current ET trends might contribute to the prediction of the Earth's runoff changes, and to the introduction of water management strategies.

Globally, ET has shown a significant upward trend over the 32-year period of 1982–2013, mainly driven by vegetation greening and rising atmosphere moisture demand [6]. It has been mainly caused by increases in transpiration from vegetation and the vaporization of intercepted rainfall from vegetation [7]. An increase in global terrestrial ET was also

reported for the period 1982–2011, as estimated by different remote sensing-based physical models, machine-learning algorithms, and land surface models [8]. Despite the overall increasing trend, decreasing ET trends were also observed in shorter periods of time. For example, it was reported that global annual evapotranspiration declined due to the limited moisture supply from 1998 to 2008 [9]. Additionally, a long-term (1950–2017) relative decline in evapotranspiration, accompanied by increasing runoff, was found in 27% of the global land areas, which was explained by a reduction in surface conductance [10]. Apart from long-term changes observed globally, the strongly regional and temporal differentiation of ET trends are evidenced, as proven for central Europe and central North America [11], and for the north-eastern United States [12]. For the period 1980–2010, large-scale increases in ET were observed in south-eastern China, while decreases in ET occurred over the north-east [13]. Other studies conducted over the 71-year period from 1948 to 2018 confirmed that ET exhibited an increasing trend over almost 90% of the territory of China [14].

In most of Europe, ET increased in response to land use (mainly large-scale reforestation and afforestation) and climate change, except in the Iberian Peninsula and some other parts of the Mediterranean where negative ET trends were found [15]. For example, Great Britain is becoming warmer and wetter, through which increases in precipitation and air temperature are driving increases in runoff and evapotranspiration, as proven for 1961–2015 [16]. In Germany, significant trends were observed in transpiration and evapotranspiration in the period of 1961–2019 [17]. Over European Russia, positive trends in the annual values of potential evapotranspiration were revealed for 1966–2017, the distribution of which has a strong, patchy character [18]. As projected for most of Europe, widespread and relatively uniform ET increases of around 75–125 mm are expected by the 2050s [19]. Overall, the trends in evapotranspiration exhibit wide regional differentiation, depending on varying climate and human impacts. The changes are linked to the main climatic drivers of ET that comprise precipitation, net solar radiation, air temperature, vapor pressure deficit, and wind speed. Transpiration, which is the main component of ET in forested landscapes [7,20], is dependent not only on the climate conditions, but also on the soil moisture regime, the physiological features of vegetation, and the duration of the growing season [21,22].

In Poland, only a few studies have focused on changes in ET from a long-term perspective. Based on data from 18 weather stations across Poland, an increase in the growing season reference evapotranspiration was detected in the period from 1971 to 2010 [23]. Moreover, a significant increase in the mean daily values of the summer reference ET in Poland in the same multiyear period was observed, with the potential to occur more frequently in the future [24]. Projections of changes of areal ET in the Wielkopolska Region (central-western part of Poland) indicate that the regional average increase in the annual ET is predicted to equal 45 mm, with the highest changes occurring during the winter, when comparing the control period of 1961–1990 to the projection horizon of 2061–2090 [25]. In the north-western part of Poland, significant increasing trends in the potential ET were observed during the period of 1952–2018, as investigated based on data acquired from six weather stations [26]. In this area, particularly high increases were detected during the spring and summer months, explained by a significant increase in air temperature and a decrease in relative humidity, marking the end of the 20th century and the start of the 21st century.

While the above-mentioned studies investigated the actual, potential, or reference ET trends from selected weather stations' data across Poland, none identified country-scale spatial–temporal patterns of ET derived from the satellite-based or reanalyzed data covering the whole territory of Poland. Hence, undertaking such research can bridge the gap and improve the understanding of the ongoing ET changes. This might provide insight into the hydrological implications that result from the ET variations helping to manage the water resources at the country and regional scales. This paper uses well-validated, satellite-based Global Land Evaporation Amsterdam Model (GLEAM) data that comprise

spatially continuous estimates of terrestrial evaporation and its main components [27–29]. For the first time, ET is quantified throughout the recent 41-year period (1980–2020), and the spatial–temporal trends are estimated across the country. New insights into the ET variability and its changes are acquired by considering the grid cell and country scale patterns. Thus far, such an approach has not been given detailed consideration with respect to the territory of Poland. Apart from investigations focusing on specific regions and based on point estimates of ET, quantitative multi-year studies incorporating spatial–temporal characteristics have not been reported.

The key scientific questions that need to be answered in this study are the following:

(1) Is the ET across Poland increasing or decreasing at annual and monthly time scales, and, if this is the case, what is the magnitude of such temporal trends?
(2) Which components of ET are contributing to the country-scale inter-annual trend?
(3) What are the monthly spatial patterns of the ET trends and regions of significantly increasing/decreasing ET?

It is hypothesized that the annual and monthly ET has remarkably increased in the past four decades, and that extremely dry and warm years have led to a high evaporation ratio, defined as the ratio between the actual terrestrial evaporation and precipitation. It is also hypothesized that the ET trends are regionally differentiated, with the highest trend rates occurring in the summer months.

2. Materials and Methods

2.1. Basic Geographical Characteristics of Poland

Poland is located in the central part of Europe. The area of the country stretches from 54.83° N to 49.00° N and from 14.18° W to 24.15° W. The land area of the country covers an area of 311,888 km^2. While the average elevation is approximately 170 m a.s.l., the relief is characterized by significant diversity. The lowest point is located in Żuławy Wiślane (−1.8 m a.s.l.) at the Baltic coast in northern Poland, and the highest peaks are in the Tatras Mountains (Rysy 2499 m a.s.l.) in the south. Lowlands (0–300 m a.s.l.) dominate and cover 91% of the country's area. Highlands (300–500 m above sea level) occupy 6%, while mountains (above 500 m above sea level) occupy only 3%. As much as 99.7% of the country's area constitutes the drainage basin of the Baltic Sea, which consists of the Vistula River Basin (53.7%), Oder River Basin (33.9%), and the river basins draining directly to the Baltic Sea (12.1%). A large part of the country (from the 14th to approximately 20–22 meridians) is influenced by a humid, temperate (Cfb) climate [30]. The rest of the area to the east and the mountainous parts to the south are classified as a snowy, humid climate (Dfb) with a warm summer. The highest annual precipitation total of approximately 1600 mm/y occurs in the Tatra Mountains, while the lowest, below 500 mm/y, concern the central, lowland part of the country. The average air temperature in the months from April to October ranges from 9.3 °C in the mountains to 14.9 °C in the midwest lowland, with a country-wide average of 13.8 °C. The land use is dominated by agricultural land (60%) and forests (33%), while the rest of the territory is covered by artificial surfaces (6%) and other categories (1%) (Figure 1).

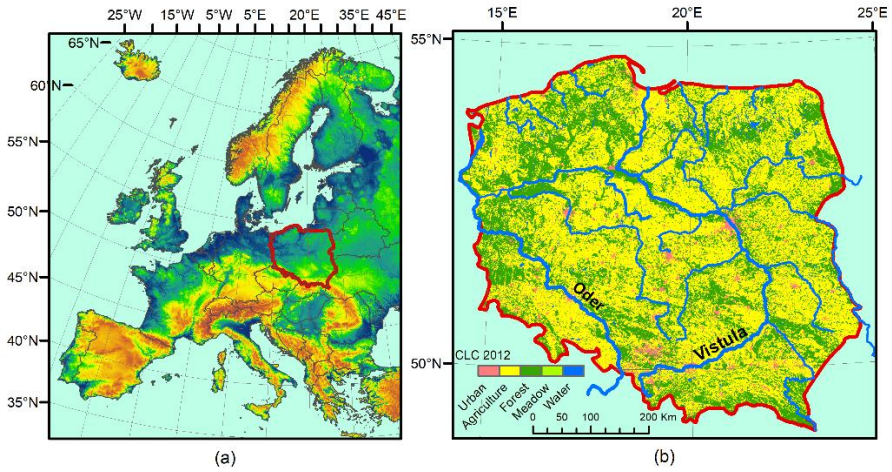

Figure 1. (**a**) Geographic location of the study area. (**b**) Land use according to CLC 2012 acquired from https://land.copernicus.eu, accessed on 7 June 2021.

2.2. Data

In this study, the satellite-based GLEAM (https://www.gleam.eu, accessed on 20 March 2021) dataset was used for detecting the magnitude and trends in terrestrial evaporation for 1980–2020. Driven by remote sensing data, GLEAM provides estimates of different components of land evaporation at a resolution of 0.25° × 0.25°, including transpiration (Et), vaporization of intercepted rainfall from vegetation (Ei), evaporation from the bare soil (Eb), snow sublimation (Es), and open-water evaporation (Ew). Version 3.5a is derived from the reanalysis of net radiation, air temperature, satellite and gauge-based precipitation, satellite-based vegetation optical depth (VOD), ESA-CCI (European Space Agency Climate Change Initiative) soil moisture, and snow water equivalent [27,28]. Changes in land cover are derived from the MEaSUREs Vegetation Continuous Fields dataset [31]. In this study, the monthly values of terrestrial evaporation were acquired and extracted for the territory of Poland. Moreover, the annual values of evaporation components (Et, Ei, Eb, Es, and Ew) were also acquired within the same spatial domain consisting 1056 grid cells. It is worth mentioning that spatial–temporal ET patterns might be captured by different regional and global ET products [32]. The GLEAM ET dataset belongs to the sophisticated land surface model group, which has an acceptable accuracy when compared to the benchmark ET values [33]. It has been recently used as a diagnostic dataset to investigate the global ET trends [34], to identify best-performing evaporation datasets [35], and to improve the structure of a simple conceptual rainfall–runoff model [36]. The key distinguishing features of these data are the multi-year observation period (1980–2020), the availability of five pieces of terrestrial evaporation component data, and the long-term satellite surface soil moisture and phenology observations assimilated into the GLEAM model.

For the analysis of the climate conditions, the air temperature and precipitation dataset was employed for 1980–2020 from version 23.1e of the station-based E-OBS gridded dataset (https://www.ecad.eu, accessed on 9 October 2021), available from the European Climate Assessment and Dataset Project [37]. It comprised daily values of precipitation (P) and air temperature (T) acquired from a regular latitude/longitude grid of 0.25° × 0.25°. From the daily gridded values, the country scale, annual air temperature, and precipitation estimates were calculated. Due to E-OBS uncertainties caused by gauge measurement errors, lack of wind corrections, and possible station relocations [38], the areal precipitation averages are considered to be underestimated [39,40]. To overcome the underestimation of the precipitation data available, a correction factor was applied to the annual precipitation totals derived from the E-OBS data. The correction factor results from the linear relationship between the E-OBS data ($P_{E\text{-}OBS}$) and the G2DC-PL+ data (P_{G2DC+}), a gridded 2 km daily climate dataset for the Polish territory, which is corrected for snowfall and rainfall under-catch and spans until 2019 [41,42]. The relationship is represented by the equation $P_{G2DC+} = 1.2 \times P_{E\text{-}OBS}$

established for the period 1980–2019. The value of the Pearson's correlation coefficient is 0.996, which confirms the strong linear relationship between the two variables. Thus, the $P_{E\text{-}OBS\text{-}corrected}$ value of the corrected E-OBS precipitation is estimated from the following equation: $P_{E\text{-}OBS\text{-}corrected} = 1.2 \times P_{E\text{-}OBS}$, where annual values of $P_{E\text{-}OBS}$ are acquired for the period 1980–2020. The corrected values of annual precipitation totals were used to calculate the values of the evaporation ratio, defined as a ratio of the actual evaporation over a given area to the precipitation falling on that area [43]. Then, the annual precipitation and air temperature time series were tested for the presence of trend, as explained in Section 2.3.

2.3. Methods

The non-parametric Mann–Kendall (MK) test [44,45] was applied for detecting trends in time series of terrestrial evaporation, precipitation, and air temperature data. It is widely applied test to analyze the hydro-meteorological time series [46]. Here, it was used to test the null hypothesis of no trend, H_0, against the alternative hypothesis, H_1, where there is an increasing or decreasing monotonic trend. The test statistic S is defined as

$$S = \sum_{k=1}^{n-1} sgn(x_j - x_k) \tag{1}$$

where x_j and x_k are the annual values in years j and k, $j > k$, respectively, n is the length of the time series, and

$$sgn(x_j - x_k) = \begin{cases} 1 & if\ (x_j - x_k) > 0 \\ 0 & if\ (x_j - x_k) = 0 \\ -1 & if\ (x_j - x_k) < 0 \end{cases} \tag{2}$$

The S statistic is approximately normally distributed when $n \geq 8$, with a mean of 0 and the variance of statistics S, σ^2, given as

$$\sigma^2 = [n(n-1)(2n+5)]/18 \tag{3}$$

The standardized test statistic Z is computed by

$$Z = \begin{cases} (S-1)/\sigma & if\ S > 0 \\ 0 & if\ S = 0 \\ (S+1)/\sigma & if\ S < 0 \end{cases} \tag{4}$$

For the country scale, annual time series of precipitation, air temperature, terrestrial evaporation, and its components, the trends were tested at a significance level of $\alpha = 0.05$. For $\alpha = 0.05$, the null hypothesis is accepted when $-1.960 \leq Z \leq 1.960$ (no significant trend), while it is rejected when $Z < -1.960$ (significant decreasing trend) or when $Z > 1.960$ (significant increasing trend). Thus, the trend is significant if the null hypothesis cannot be accepted. For the monthly terrestrial evaporation time series in a multi-year period 1980–2020, the significance level $\alpha = 0.1$ was assumed. For the assumed $\alpha = 0.1$, the null hypothesis is accepted when $-1.645 \leq Z \leq 1.645$ (no significant trend), while it is rejected when $Z < -1.645$ (significant decreasing trend) or when $Z > 1.645$ (significant increasing trend). For the computation of the magnitude (slope) of an existing trend (as change per year), the directional coefficient β expressed by the Theil–Sen estimator [47,48] is calculated by the formula:

$$\beta = Median\left((x_j - x_k)/(j-k)\right) \tag{5}$$

A positive value of β signals an increasing trend, and a negative value of β indicates a decreasing trend. In case the change is not statistically significant, but shows an inclination, it is called a tendency. The Climate Data Toolbox (CDT) for MATLAB [49] was used to calculate the MK test statistic (Z) and the p-values.

For the shift-type changes, the terrestrial evaporation time series were partitioned into two subseries by minimizing the sum of the residual (squared) error of each subset from

its local mean, and finally returning the index, which, in this case, is the year in which the change occurs. The change point was identified for the country-scale time series of annual ET sums by using the MATLAB function "findchangepts". In the analysis performed here, a complete 41-element ET time series was divided into subperiods of differing length, consisting of 27 and 14 records covering the years 1980–2006 and 2007–2020, respectively. Finally, the Kruskal–Wallis test was applied to test for statistically significant differences between the subseries in two selected subperiods [50,51] by using HYDROSPECT software [52]. This test is a non-parametric test that compares mean ranks (i.e., medians). For this test, the null hypothesis is that the subseries medians are equal, versus the alternative that there is a difference between them. Under the null hypothesis of equal subperiod means, the statistic follows the Chi-square distribution. The Kruskal–Wallis test statistic is calculated as

$$H = \frac{12}{n(n+1) - T} \sum_{i=1}^{N} n_i (m_i - m)^2 \quad (6)$$

$$T = \frac{1}{n-1} \sum t_j^3 - t_j \quad (7)$$

where n is the series length, m the global mean of ranks, N denotes the number of subperiods, n_i is the number of values in the i-th subperiod, m_i is the mean rank for the i-th subperiod, T is the "tie correction", and t_j denotes the number of ties in subsequent tie groups [50]. The value of T for $t = 1$ is equal to 0. The Kruskall–Wallis test was also applied to the 41-element monthly ET time series partitioned into two 27- and 14-element subseries, as a split series of annual ET totals.

3. Results

3.1. Country Scale, Inter-Annual Terrestrial Evaporation over the Period 1980–2020

Figure 2 shows the course of the country scale of the annual sum of terrestrial evaporation comprised of its components in the analyzed period 1980–2020. It is within the range of 409–491 mm, and the multi-year average (1980–2020) equals 455 mm. The largest share in ET is Et (78%), and the second quantitatively important component is Ei (17%). The other contributions, Eb, Es, and Ew, have much smaller shares, i.e., 2%, 1%, and 2%, respectively. The annual ET shows an increasing trend of 1.36 mm/y in response to the slightly increasing tendency in precipitation (P) and the significant increase in air temperature (Figure 3a). The increasing ET is the result of the statistically significant increases in Et, Ei, and Ew, which outweigh the decreasing trend in Eb and the decreasing tendency in Es (Figure 3a,b). Noteworthy are the high values of Es in 1995 and 2006, which presumably were caused by particularly long-lasting snow cover, usually occurring from mid-December to the end of April. The multi-year rate of change of Et, Ei, Eb, Es, and Ew is equal to 0.84, 0.61, −0.04, −0.08, and 0.03 mm/y, respectively.

A shift-type temporal change of annual ET occurred in 2007, as detected by the change point analysis (Figure 3c). The Kruskal–Wallis test confirmed the significance of the difference between the median values of ET in the two subperiods. It shifted from 449 mm in the subperiod of 1980–2006 to 480 mm in the subperiod of 2007–2020. Additionally, the mean annual ET changed from 444 mm to 476 mm. There was also a significant shift-type change in the components of terrestrial evaporation, and this concerns transpiration, interception loss, and open-water evaporation. The average evaporation ratio (ET/P) in the period before the change was 65%, while after the change, it increased by 3% to a value of 68%. However, in particularly wet years, it was much lower, while in dry years, it reached very high values. For example, in the wet years of 2010 and 2017, it was equal to 50% and 56%, respectively, while in dry years, it was far above the long-term average, reaching 95% in 1982, 84% in 2015, and 87% in 2018.

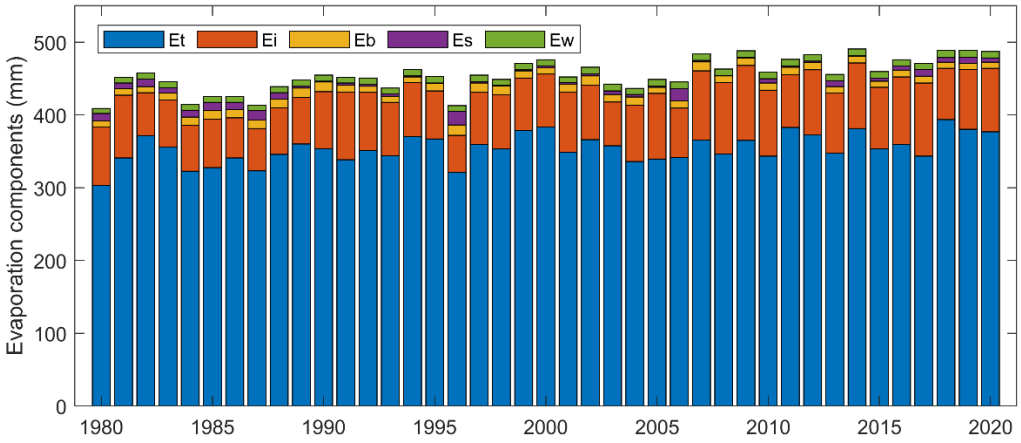

Figure 2. Annual terrestrial evaporation (ET) over Poland in 1980–2020, composed of transpiration (Et), interception loss (Ei), open-water evaporation (Ew), snow sublimation (Es), and bare soil evaporation (Eb).

Thus, atmospheric conditions, represented here by temperature and precipitation, control extreme ET values affecting the range of anomalies. In this work, precipitation and temperature are considered as selected ET drivers, although it should be noted that other factors, such as wind, solar radiation, and air humidity, can also play an important role. Except for climatological–meteorological conditions, other features such as hydrogeological, topographical, and physiological characteristics can also be critical.

3.2. Country-Scale, Monthly Terrestrial Evaporation over the Multi-Year Period 1980–2020

Figure 4 shows the course of the country-scale, monthly ET in the analyzed period 1980–2020. Statistically significant increasing trends occurred in summer and early fall, from June to October. In winter, an increase took place in January (0.08 mm/y). In the remaining months, the changes were not significant. The highest increases occurred in June (0.37 mm/y), July (0.30 mm/y), and August (0.21 mm/y). Much smaller changes concerned the months of September (0.13 mm/y) and October (0.05 mm/y).

An annual cycle is exhibited by ET, with the highest values in the summer season (June–August) and the lowest values in the winter season (November–February), as shown in Figure 5. Comparing the two subperiods, the second subperiod (2007–2020) is marked by a clear increase in ET in June (from 73 mm to 81 mm), July (from 77 mm to 84 mm), and August (from 63 mm to 68 mm) (Figure 5b). In these months, the increase in ET reached on average of 9%. The shift type changes in ET were statistically significant at $\mapsto = 0.05$ in January and in all months from June to September, as determined by the Kruskal–Wallis test. The same is true for ET totals in the months from April to October.

3.3. Monthly and Annual Spatial Patterns of Terrestrial Evaporation

Figure 6 shows the mean monthly spatial patterns of ET for 1980–2020. In December, January, and February, the values were the lowest. From March on, throughout April and May, they gradually increased, reaching the highest values in June, July, and August. Then, starting from September, they gradually decreased, reaching the lowest values in the winter months. Throughout the whole year, the highest monthly ET occurred in the south, and it concerned the mountainous, forested area. The area with relatively high ET values was also located in the western and northwestern part of Poland, where there were dense forest complexes. The lowest monthly ET were characteristic for the central zone, stretching from west to east.

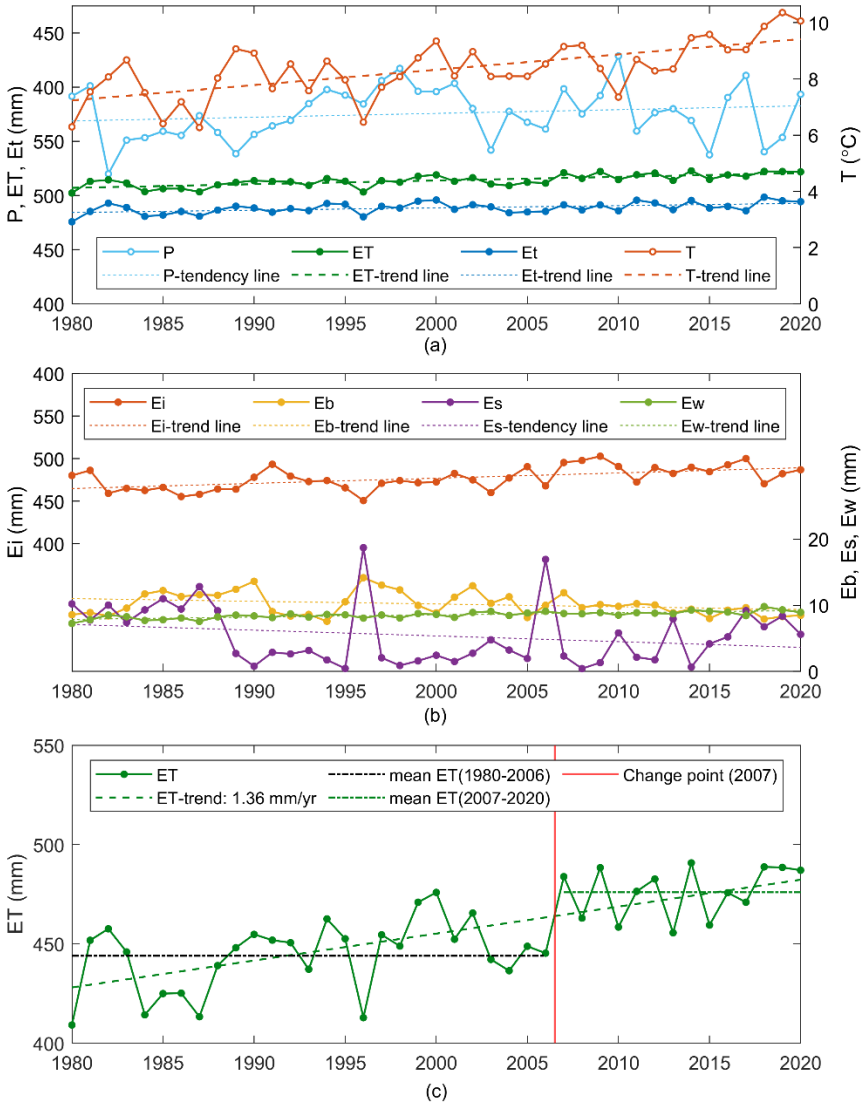

Figure 3. (**a**) Changes in annual precipitation (P), air temperature (T), terrestrial evaporation (ET), and transpiration (Et) in the multi-year period 1980–2020. (**b**) Changes in evaporation from interception (Ei), evaporation from bare soil (Eb), sublimation (Es), and evaporation from water (Ew) in the multi-year period 1980–2020. (**c**) Terrestrial evaporation (ET) in two subperiods (1980–2006 and 2007–2020), separated by a change point in 2007. The presence of a trend is determined at the significance level of $\alpha = 0.05$.

To check if there was a trend in monthly ET, 41-element time series were prepared for each grid cell for each month. Then, the Mann–Kendall test was applied. The results are presented in Figure 7 and Table 1. A statistically significant increasing trend occurred in many grid cells in June–September, covering 96% of the country's territory in June (Figure 7f), 89% in July (Figure 7g), 84% in August, and 75% in September. An increasing ET trend was also observed in 59% of the territory of Poland in January (Figure 7a).

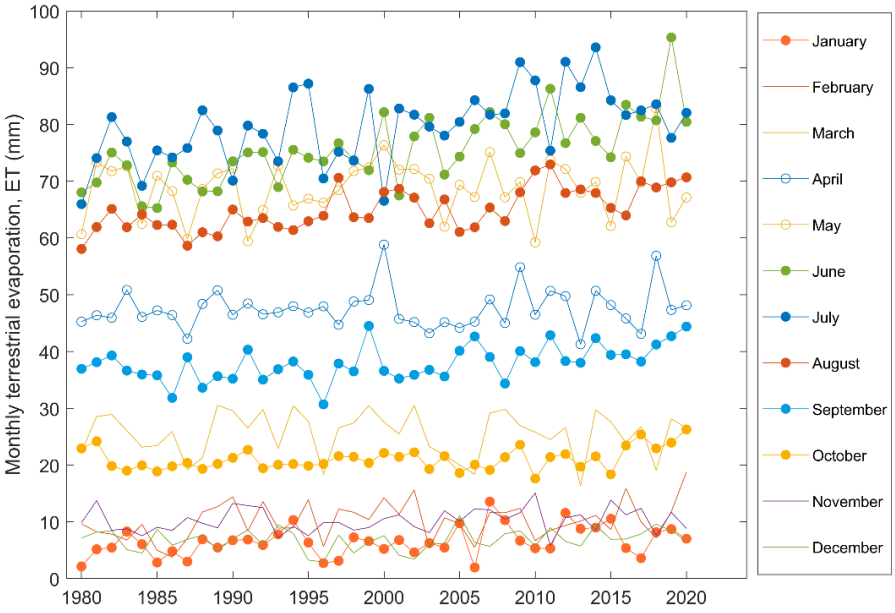

Figure 4. Monthly time series of terrestrial evaporation (ET) over Poland in 1980–2020. Statistically significant trends are indicated by filled markers. The presence of a trend is determined at a significance level of $\alpha = 0.05$.

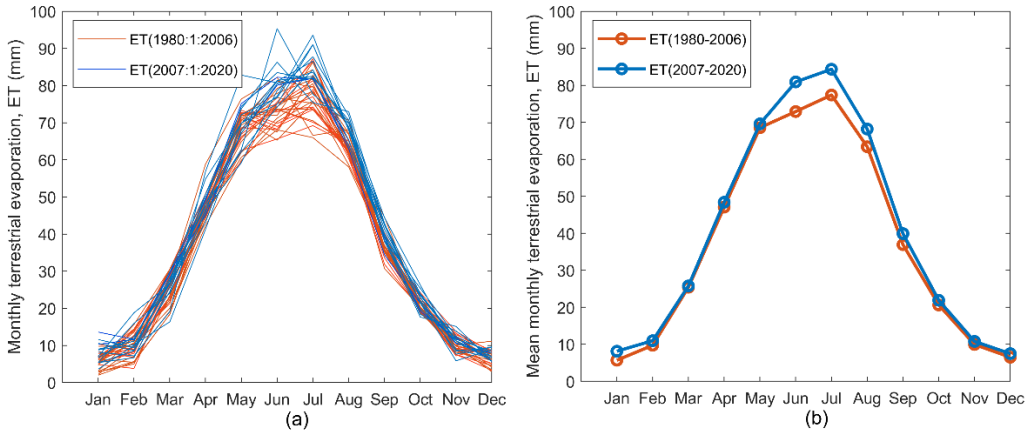

Figure 5. (**a**) Monthly terrestrial evaporation (ET). (**b**) Mean monthly terrestrial evaporation (ET) for subperiod 1 (1980–2006) and subperiod 2 (2007–2020). The ET values are averaged over the territory of Poland.

The trend rate of ET over the 41-year period was the highest in June, July, and August (Figure 8). In June, 63% of the territory experienced a trend rate of 0.20–0.39 mm/y, 29% had a trend rate of 0.40–0.59 mm/y, 2% was marked by a highest trend rate of 0.60–0.79 mm/y, and 2% was marked by a rate of 0.01–0.19 mm/y (Figure 8f). In July, the trend rate of 0.20–0.39 mm/y dominated as well, covering 57% of the territory, while the rate of 0.01–0.19 mm/y (either trend or tendency) was observed in 22% of the territory, a trend rate of 0.40–0.59 mm/y concerned 17% of the territory, and 0.60–0.79 mm/y concerned 2% of the territory. The remaining 2% of the territory experienced a slight decreasing tendency of −0.19–0 mm/y. The contribution of particular trend rate classes changed in August; 46% of the country had a trend or tendency rate of 0.01–0.19 mm/y, while the rates of 0.20–0.39 mm/y, 0.40–0.59 mm/y, and −0.19–0.00 mm/y concerned 43%, 9%, and 2% of the country, respectively. While the rising ET trend dominated in the summer, a slight downward trend or tendency was observed across the country during the spring months.

This applied to the months of March, April, and May when the changes were in the range of −0.19–0 mm/y, and they covered 68%, 48%, and 42% of the country territory, respectively.

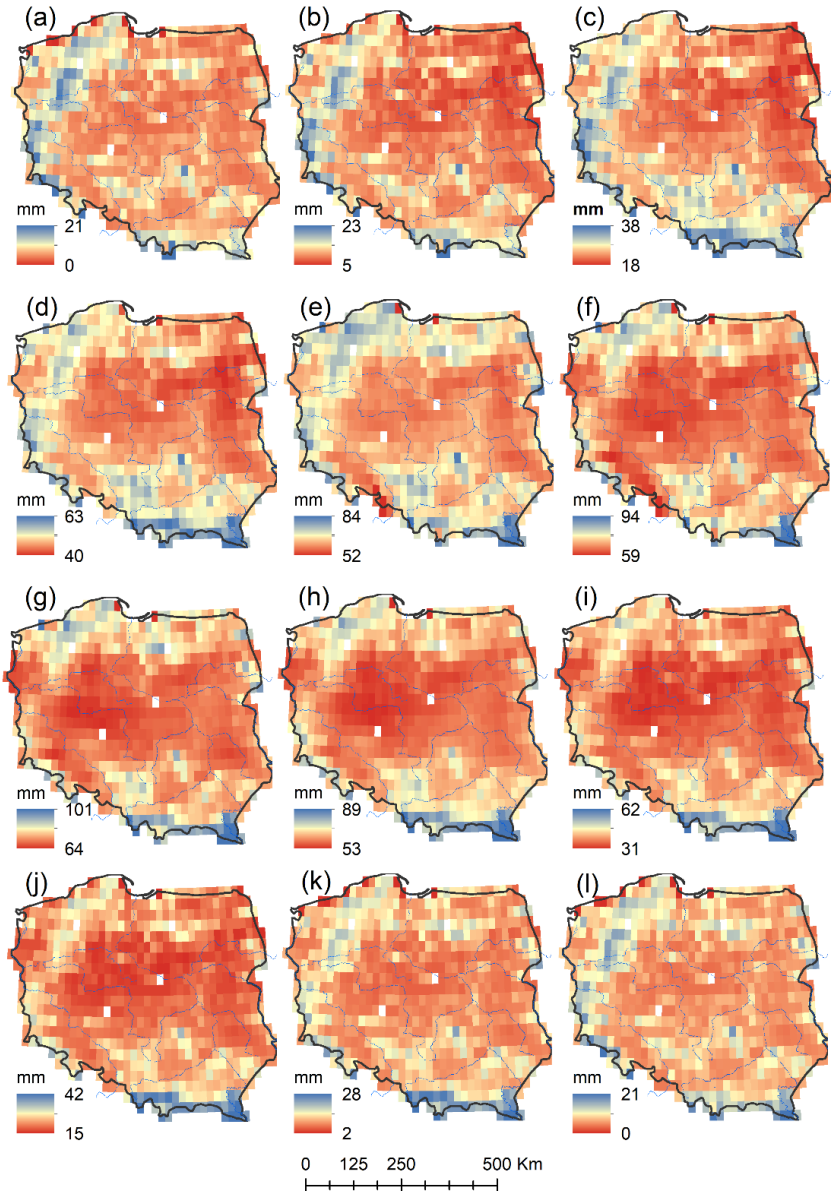

Figure 6. Spatial patterns of mean monthly ET during 1980–2020 for: (**a**) January, (**b**) February, (**c**) March, (**d**) April, (**e**) May, (**f**) June, (**g**) July, (**h**) August, (**i**) September, (**j**) October, (**k**) November, and (**l**) December.

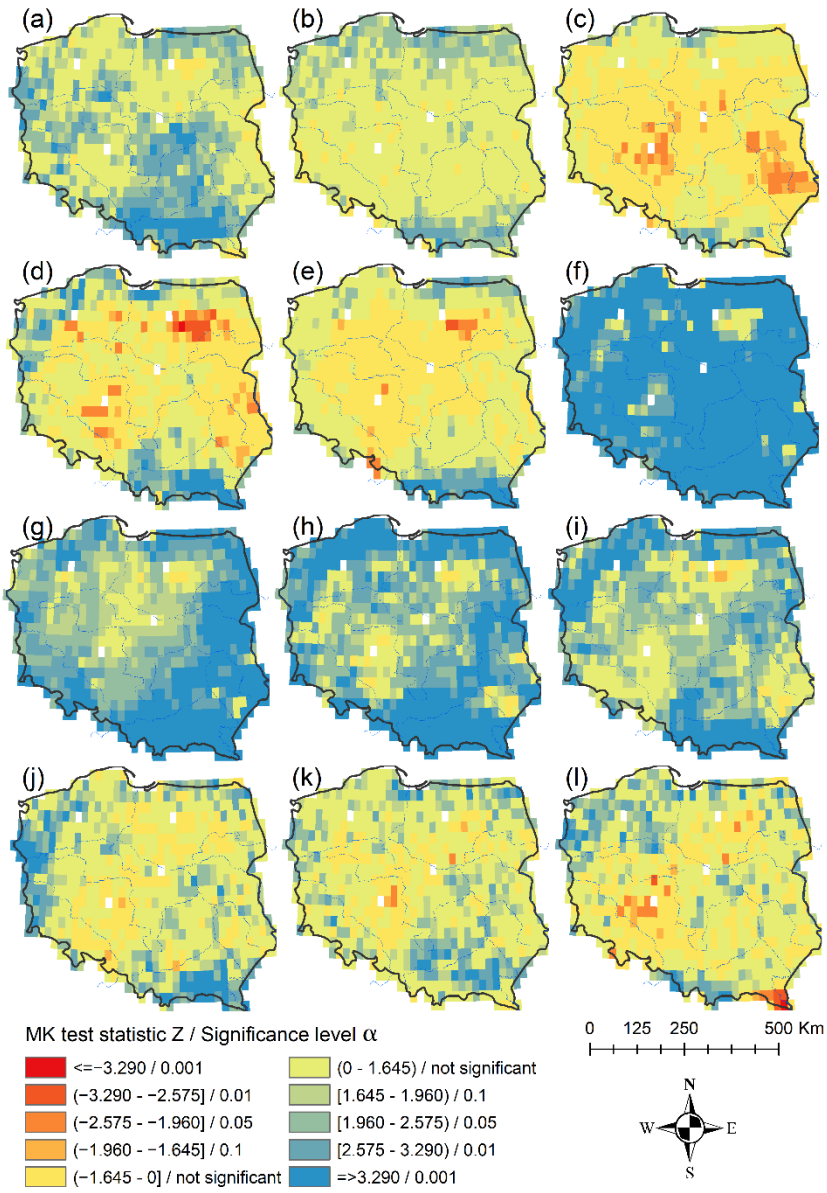

Figure 7. Mann–Kendall test results of ET trend detection over Poland at significance levels of ↦ 0.001, 0.01, 0.05, and 0.1 in the period 1980–2020 for: (**a**) January, (**b**) February, (**c**) March, (**d**) April, (**e**) May, (**f**) June, (**g**) July, (**h**) August, (**i**) September, (**j**) October, (**k**) November, and (**l**) December. Red and orange grid cells indicate a decreasing trend, light green and blue grid cells show an increasing trend, whereas yellow and yellowish green indicate no trend detected. Four grid cells with no data are shown in white.

Table 1. Percent of the country area with decreasing or increasing ET trends, or without changes in ET detected. The presence of a trend is determined at a significance level of $\alpha = 0.1$.

Month	Percent of Area with Increasing ET Trend %	Percent of Area with Decreasing ET Trend %	Percent of Area with No Changes in ET %
January	58	0	42
February	30	0	70
March	5	9	86
April	22	7	71
May	16	2	82

Table 1. *Cont.*

Month	Percent of Area with Increasing ET Trend %	Percent of Area with Decreasing ET Trend %	Percent of Area with No Changes in ET %
June	96	0	4
July	89	0	11
August	84	0	16
September	75	0	25
October	35	0	65
November	31	0	69
December	24	4	72

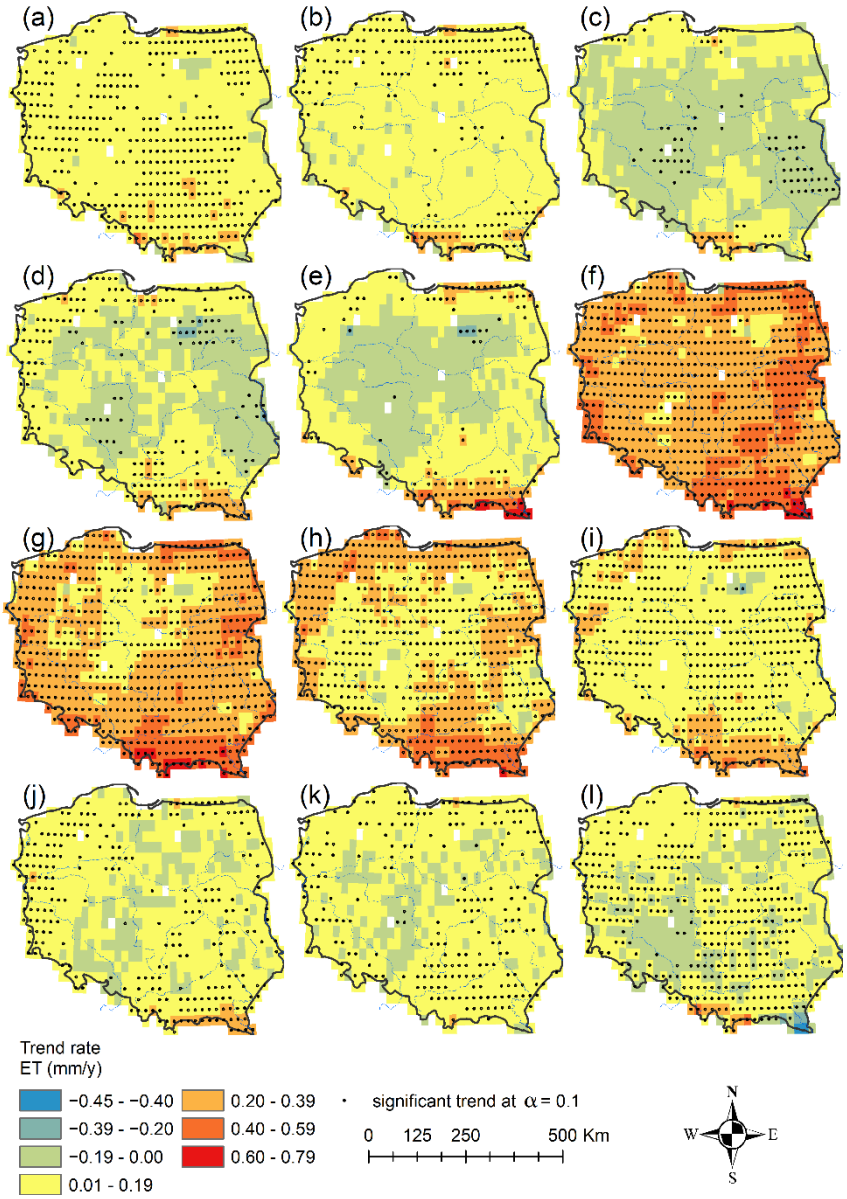

Figure 8. Trend rate of monthly terrestrial evaporation (ET) in the multi-year period 1980–2020 for: (**a**) January, (**b**) February, (**c**) March, (**d**) April, (**e**) May, (**f**) June, (**g**) July, (**h**) August, (**i**) September, (**j**) October, (**k**) November, and (**l**) December.

Finally, the spatial patterns of the annual ET were elaborated (Figure 9). Overall, the highest ET values occurred in the southern mountainous part of the country (Figure 9a),

determined by the relatively high precipitation totals and the land use dominated by forests. The land strips in the north-west and west were also marked by relatively high ET values, associated with the presence of dense forest complexes in this area. Much lower ET occurred in the central part of the country, but also in the south-western, north-eastern, and eastern parts of the country, where agricultural fields have a large share in the land use. The comparison of ET in the two selected subperiods showed that subperiod 2 (2007–2020) had significantly higher ET values than subperiod 1 (1980–2006) (Figure 9b,c). The minimum ET values observed across the country were 35 mm higher, and the maximum values increased by 63 mm. The annual ET difference in the range of 0.1–20 mm/y was detected in the zone spreading from the south-west to the north-east, while much higher differences in the south reached, locally, up to 115 mm (Figure 9e). Only five grid cells were characterized by an ET decrease of up to 3% (Figure 9f), of which only one cell had a statistically significant decrease (Figure 9d). A total of 87% of the country experienced an increase of 1–10% ET, while a 11–22% increase was characteristic for the rest of the area (Figure 9f). Overall, the statistically significant increase in annual ET concerned 90% of the country's territory (Figure 9d).

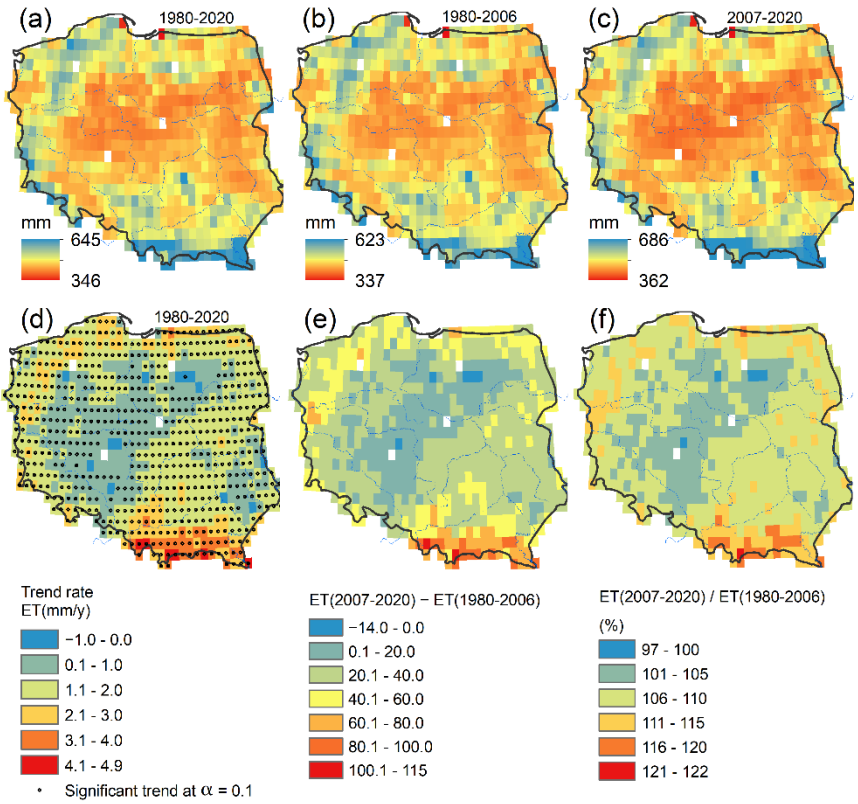

Figure 9. (**a**) Annual terrestrial evaporation (ET) in the multi-year period 1980–2020. (**b**) Annual terrestrial evaporation (ET) in the subperiod 1980–2006. (**c**) Annual terrestrial evaporation (ET) in the subperiod 2007–2020. (**d**) Trend rate of annual ET in the multi-year period 1980–2020. (**e**) Anomalies in annual ET detected as a difference between ET (2007–2020) and ET (1980-2006). (**f**) Anomalies in annual ET detected as a ratio of ET (2007–2020) to ET (1980–2006).

4. Discussion

This study demonstrated that terrestrial evaporation has increased both at the annual and monthly time scale. This finding supports the hypothesis that terrestrial evaporation has remarkably increased in the past four decades. The ET increase was caused by increases in transpiration, interception loss, and open-water evaporation, partially counteracted by bare soil evaporation and sublimation decreases. The increasing trends in transpiration (0.87 mm/y) and interception loss (0.68 mm/y) have the largest contribution to the ET

changes. They are presumably driven by increases in the vegetation leaf area index, dominated by greening [6]. In Poland, greening has recently been confirmed by increasing NDVI trends, showing that 59% of the country has been greening continuously since the 1980s and that it has a widespread character [53]. This process affected over 44% of 1980s agricultural land and 87% of 1980s non-agricultural land. In total, this concerned nearly 60% of the country's area. Thus, the intensified greening all over the country coincides with the increase in terrestrial evaporation detected in this study; 81% of the territory is marked by an ET increase of 0.1–2 mm/y (trend or tendency), while 17% has a change of 2.1–4.9 mm/y. Only 2% of the territory has a decreasing tendency. To conclude, most of Poland has experienced an increasing ET trend in the last four decades, and the evaporation ratio was extraordinarily high in dry and warm years, such as 1982, 2015, and 2018.

The follow-up hypothesis is also confirmed; ET trends are regionally differentiated, with the highest multi-year trend rates occurring in June, July, and August, equaling, on average, 0.35 mm/y, 0.30 mm/y, and 0.22 mm/y, respectively. These are signals of an accelerated, more intense water cycle. The main implication of this finding is that increasing ET rates might have a great impact on the other components of the water cycle. If the observed ET trends continue, the associated changes in water budget components might present challenges for water managers at country and regional scales.

In this study, a well-validated satellite-based GLEAM dataset was used for analyzing ET dynamics for 1980–2020. To the best of the author's knowledge, this is the first study for the Polish territory that gives country-scale estimates of terrestrial evaporation over the last four decades. This enabled the analysis of total terrestrial evaporation and its components in the multi-year period. This study explained the relative contribution of each ET component, revealing the dominant role of transpiration and interception loss in the terrestrial evaporation. The mean annual ET of 455 mm/y is comparable to the ET of 442 mm/y, which was estimated for the whole of Europe [7]. However, the contribution of transpiration to the ET differs (69% for Europe and 78% for Poland). Additionally, clear differences concern the role of interception loss and bare soil evaporation. In this study, interception loss (77 mm/y) contributed in the amount of 17% to the ET (455 mm/y), which is almost double the amount estimated for Europe (9%). In turn, the bare soil evaporation contribution was found to be only 2%, while for Europe, it was found to be 21%. Such divergent results might be due to differences in model-dependent partitioning approaches, datasets forcing the ET models, the differences in climatic and land surface characteristics, and vegetation morphological attributes. The implication is that the relationships between particular components of ET should be further explored in a future study. It is worth noting that the multi-year ET average (455 mm) determined in this study is relatively consistent with earlier estimates for the territory of Poland; it is only slightly higher than estimates for the Oder River basin (454 mm) and for the Vistula River basin (432 mm) reported in 1950s [54]. The discrepancy is very low and may be due to the difference in source data (derived from the water budget) and a different period (1920–1940). Much higher ET values (553 mm) were signaled for 1961–1990 in the Wielkopolska region located in central and western Poland [25]. Such contrasting results are probably due to differences in applied methods and different sets of variables forcing the ET models from which areal ET values are derived. Moreover, this region cannot be treated as representative for the whole territory of Poland.

5. Conclusions

To conclude, this study evaluated the magnitude and multi-year trends in terrestrial evaporation and its components across Poland. Benefitting from the novel satellite observations assimilated to GLEAM, together with the reanalysis data used as the model forcing, it was found that most of Poland experienced significant terrestrial evaporation increases from 1980 to 2020. The warmer climate, along with a small precipitation increase, led to increased vegetation activity. This was revealed by increased transpiration and interception loss not compensated by a decrease in bare soil evaporation and sublimation. The en-

hanced vegetation activity was manifested by the wide-spread higher water consumption, especially during the summer months of June, July, and August. These monthly increases contributed to the annual changes in terrestrial evaporation of 1.36 mm/y. Comparing the two subperiods of 1980–2020, it was found that in the subperiod 2007–2020, the annual evaporation increased by 7% compared to the reference subperiod of 1980–2006. Further study on the quantification of terrestrial evaporation is required to explain its impacts on the changing water budget structure. This can serve as a reference for formulating a water resources management strategy in Poland.

Funding: This research was funded by the Faculty of Geography and Regional Studies, University of Warsaw, Poland, grant no. SWIB55/2021, and by the University of Warsaw, Poland, "Excellence Initiative–Research University" program, Action IV.3.1, grant no. BOB-661-519/2021.

Institutional Review Board Statement: Not applicable.

Informed Consent Statement: Not applicable.

Data Availability Statement: All the data used during this study are available at locations cited in the acknowledgements section.

Acknowledgments: The author thanks the editors and reviewers for their insightful comments and suggestions. The author acknowledges the GLEAM dataset (version 3.5a), which is available at https://www.gleam.eu (accessed on 20 March 2021). The author also acknowledges the E-OBS dataset from the ECA&D project (http://www.ecad.eu, accessed on 9 October 2021); version 23.1e of the dataset was downloaded from the Copernicus Climate Change Service (https://surfobs.climate.copernicus.eu/dataaccess/access_eobs.php) (accessed on 9 October 2021). The CORINE Land Cover was downloaded from the Copernicus Land Monitoring Service (https://land.copernicus.eu), European Union, European Environment Agency (EEA) (accessed on 7 June 2021). The author also acknowledges the G2DC-PL+ dataset openly available from the 4TU Centre for Research Data (https://doi.org/10.4121/uuid:a3bed3b8-e22a-4b68-8d75-7b87109c9feb, accessed on 16 September 2021).

Conflicts of Interest: The author declares no conflict of interest. The funder had no role in the design of the study; in the collection, analyses, or interpretation of data; in the writing of the manuscript; or in the decision to publish the results.

References

1. Miralles, D.G.; Brutsaert, W.; Dolman, A.J.; Gash, J.H. On the Use of the Term "Evapotranspiration". *Water Resour. Res.* **2020**, *56*, e2020WR028055. [CrossRef]
2. Paschalis, A.; Fatichi, S.; Pappas, C.; Or, D. Covariation of vegetation and climate constrains present and future T/ET variability. *Environ. Res. Lett.* **2018**, *13*, 104012. [CrossRef]
3. Wang-Erlandsson, L.; Van Der Ent, R.J.; Gordon, L.J.; Savenije, H.H.G. Contrasting roles of interception and transpiration in the hydrological cycle—Part 1: Temporal characteristics over land. *Earth Syst. Dyn.* **2014**, *5*, 441–469. [CrossRef]
4. Laguë, M.M.; Pietschnig, M.; Ragen, S.; Smith, T.A.; Battisti, D.S. Terrestrial Evaporation and Global Climate: Lessons from Northland, a Planet with a Hemispheric Continent. *J. Clim.* **2021**, *34*, 2253–2276. [CrossRef]
5. Zhan, S.; Song, C.; Wang, J.; Sheng, Y.; Quan, J. A Global Assessment of Terrestrial Evapotranspiration Increase Due to Surface Water Area Change. *Earth's Futur.* **2019**, *7*, 266–282. [CrossRef]
6. Zhang, K.; Kimball, J.S.; Nemani, R.R.; Running, S.W.; Hong, Y.; Gourley, J.J.; Yu, Z. Vegetation Greening and Climate Change Promote Multidecadal Rises of Global Land Evapotranspiration. *Sci. Rep.* **2015**, *5*, 15956. [CrossRef]
7. Zhang, Y.; Peña-Arancibia, J.L.; McVicar, T.R.; Chiew, F.H.S.; Vaze, J.; Liu, C.; Lu, X.; Zheng, H.; Wang, Y.; Liu, Y.Y.; et al. Multi-decadal trends in global terrestrial evapotranspiration and its components. *Sci. Rep.* **2016**, *6*, 19124. [CrossRef]
8. Pan, S.; Pan, N.; Tian, H.; Friedlingstein, P.; Sitch, S.; Shi, H.; Arora, V.K.; Haverd, V.; Jain, A.K.; Kato, E.; et al. Evaluation of global terrestrial evapotranspiration using state-of-the-art approaches in remote sensing, machine learning and land surface modeling. *Hydrol. Earth Syst. Sci.* **2020**, *24*, 1485–1509. [CrossRef]
9. Jung, M.; Reichstein, M.; Ciais, P.; Seneviratne, S.I.; Sheffield, J.; Goulden, M.L.; Bonan, G.; Cescatti, A.; Chen, J.; De Jeu, R.; et al. Recent decline in the global land evapotranspiration trend due to limited moisture supply. *Nature* **2010**, *467*, 951–954. [CrossRef]
10. Wang, R.; Gentine, P.; Yin, J.; Chen, L.; Chen, J.; Li, L. Long-term relative decline in evapotranspiration with increasing runoff on fractional land surfaces. *Hydrol. Earth Syst. Sci.* **2021**, *25*, 3805–3818. [CrossRef]
11. Teuling, A.J.; Hirschi, M.; Ohmura, A.; Wild, M.; Reichstein, M.; Ciais, P.; Buchmann, N.; Ammann, C.; Montagnani, L.; Richardson, A.D.; et al. A regional perspective on trends in continental evaporation. *Geophys. Res. Lett.* **2009**, *36*, L02404. [CrossRef]

12. Vadeboncoeur, M.A.; Green, M.B.; Asbjornsen, H.; Campbell, J.L.; Adams, M.B.; Boyer, E.W.; Burns, D.A.; Fernandez, I.J.; Mitchell, M.J.; Shanley, J.B. Systematic variation in evapotranspiration trends and drivers across the Northeastern United States. *Hydrol. Process.* **2018**, *32*, 3547–3560. [CrossRef]
13. Li, S.; Wang, G.; Sun, S.; Fiifi Tawia Hagan, D.; Chen, T.; Dolman, H.; Liu, Y. Long-term changes in evapotranspiration over China and attribution to climatic drivers during 1980–2010. *J. Hydrol.* **2021**, *595*, 126037. [CrossRef]
14. Zhang, F.; Geng, M.; Wu, Q.; Liang, Y. Study on the spatial-temporal variation in evapotranspiration in China from 1948 to 2018. *Sci. Rep.* **2020**, *10*, 17139. [CrossRef]
15. Teuling, A.J.; De Badts, E.A.G.; Jansen, F.A.; Fuchs, R.; Buitink, J.; Van Dijke, A.J.H.; Sterling, S.M. Climate change, reforestation/afforestation, and urbanization impacts on evapotranspiration and streamflow in Europe. *Hydrol. Earth Syst. Sci.* **2019**, *23*, 3631–3652. [CrossRef]
16. Blyth, E.M.; Martínez-de la Torre, A.; Robinson, E.L. Trends in evapotranspiration and its drivers in Great Britain: 1961 to 2015. *Prog. Phys. Geogr.* **2019**, *43*, 666–693. [CrossRef]
17. Ziche, D.; Riek, W.; Russ, A.; Hentschel, R.; Martin, J. Water budgets of managed forests in northeast germany under climate change—Results from a model study on forest monitoring sites. *Appl. Sci.* **2021**, *11*, 2403. [CrossRef]
18. Malinin, V.N.; Gordeeva, S.M.; Mitina, Y.V.; Kuleshova, A.V. Interannual variability of moistening in the European Russia. *Russ. J. Earth Sci.* **2021**, *21*, 1. [CrossRef]
19. Dezsi, Ş.; Mîndrescu, M.; Petrea, D.; Rai, P.K.; Hamann, A.; Nistor, M.M. High-resolution projections of evapotranspiration and water availability for Europe under climate change. *Int. J. Climatol.* **2018**, *38*, 3832–3841. [CrossRef]
20. Jasechko, S.; Sharp, Z.D.; Gibson, J.J.; Birks, S.J.; Yi, Y.; Fawcett, P.J. Terrestrial water fluxes dominated by transpiration. *Nature* **2013**, *496*, 347–350. [CrossRef] [PubMed]
21. Hursh, A.; Ballantyne, A.; Cooper, L.; Maneta, M.; Kimball, J.; Watts, J. The sensitivity of soil respiration to soil temperature, moisture, and carbon supply at the global scale. *Glob. Chang. Biol.* **2017**, *23*, 2090–2103. [CrossRef]
22. Liu, X.; Biondi, F. Transpiration drivers of high-elevation five-needle pines (*Pinus longaeva* and *Pinus flexilis*) in sky-island ecosystems of the North American Great Basin. *Sci. Total Environ.* **2020**, *739*, 139861. [CrossRef] [PubMed]
23. Łabędzki, L.; Bąk, B.; Smarzyńska, K. Spatio-temporal variability and trends of Penman-Monteith reference evapotranspiration (FAO-56) in 1971-2010 under climatic conditions of Poland. *Polish J. Environ. Stud.* **2014**, *23*, 2083–2091. [CrossRef]
24. Bogawski, P.; Bednorz, E. Atmospheric conditions controlling extreme summertime evapotranspiration in Poland (central Europe). *Nat. Hazards* **2016**, *81*, 55–69. [CrossRef]
25. Szwed, M. Projections of changes of areal evapotranspiration for different land-use units in the Wielkopolska Region (Poland). *Theor. Appl. Climatol.* **2017**, *130*, 291–304. [CrossRef]
26. Okoniewska, M.; Szuminska, D. Changes in potential evaporation in the years 1952–2018 in North-Western Poland in terms of the impact of climatic changes on hydrological and hydrochemical conditions. *Water* **2020**, *12*, 877. [CrossRef]
27. Martens, B.; Miralles, D.G.; Lievens, H.; Van Der Schalie, R.; De Jeu, R.A.M.; Fernández-Prieto, D.; Beck, H.E.; Dorigo, W.A.; Verhoest, N.E.C. GLEAM v3: Satellite-based land evaporation and root-zone soil moisture. *Geosci. Model Dev.* **2017**, *10*, 1903–1925. [CrossRef]
28. Miralles, D.G.; De Jeu, R.A.M.; Gash, J.H.; Holmes, T.R.H.; Dolman, A.J. Magnitude and variability of land evaporation and its components at the global scale. *Hydrol. Earth Syst. Sci.* **2011**, *15*, 967–981. [CrossRef]
29. Miralles, D.G.; Holmes, T.R.H.; De Jeu, R.A.M.; Gash, J.H.; Meesters, A.G.C.A.; Dolman, A.J. Global land-surface evaporation estimated from satellite-based observations. *Hydrol. Earth Syst. Sci.* **2011**, *15*, 453–469. [CrossRef]
30. Kottek, M.; Grieser, J.; Beck, C.; Rudolf, B.; Rubel, F. World map of the Köppen-Geiger climate classification updated. *Meteorol. Z.* **2006**, *15*, 259–263. [CrossRef]
31. Song, X.P.; Hansen, M.C.; Stehman, S.V.; Potapov, P.V.; Tyukavina, A.; Vermote, E.F.; Townshend, J.R. Global land change from 1982 to 2016. *Nature* **2018**, *560*, 639–643. [CrossRef]
32. Xu, T.; Guo, Z.; Xia, Y.; Ferreira, V.G.; Liu, S.; Wang, K.; Yao, Y.; Zhang, X.; Zhao, C. Evaluation of twelve evapotranspiration products from machine learning, remote sensing and land surface models over conterminous United States. *J. Hydrol.* **2019**, *578*, 124105. [CrossRef]
33. Chao, L.; Zhang, K.; Wang, J.; Feng, J.; Zhang, M. A comprehensive evaluation of five evapotranspiration datasets based on ground and grace satellite observations: Implications for improvement of evapotranspiration retrieval algorithm. *Remote Sens.* **2021**, *13*, 2414. [CrossRef]
34. Kim, S.; Anabalón, A.; Sharma, A. An assessment of concurrency in evapotranspiration trends across multiple global datasets. *J. Hydrometeorol.* **2021**, *22*, 231–244. [CrossRef]
35. Dembélé, M.; Ceperley, N.; Zwart, S.J.; Salvadore, E.; Mariethoz, G.; Schaefli, B. Potential of satellite and reanalysis evaporation datasets for hydrological modelling under various model calibration strategies. *Adv. Water Resour.* **2020**, *143*, 103667. [CrossRef]
36. Roy, T.; Gupta, H.V.; Serrat-Capdevila, A.; Valdes, J.B. Using satellite-based evapotranspiration estimates to improve the structure of a simple conceptual rainfall-runoff model. *Hydrol. Earth Syst. Sci.* **2017**, *21*, 879–896. [CrossRef]
37. Cornes, R.C.; van der Schrier, G.; van den Besselaar, E.J.M.; Jones, P.D. An Ensemble Version of the E-OBS Temperature and Precipitation Data Sets. *J. Geophys. Res. Atmos.* **2018**, *123*, 9391–9409. [CrossRef]
38. Lockhoff, M.; Zolina, O.; Simmer, C.; Schulz, J. Representation of precipitation characteristics and extremes in regional reanalyses and satellite-and gauge-based estimates over western and central Europe. *J. Hydrometeorol.* **2019**, *20*, 1123–1145. [CrossRef]

39. Hofstra, N.; Haylock, M.; New, M.; Jones, P.D. Testing E-OBS European high-resolution gridded data set of daily precipitation and surface temperature. *J. Geophys. Res. Atmos.* **2009**, *114*, D21101. [CrossRef]
40. Gampe, D.; Ludwig, R. Evaluation of gridded precipitation data products for hydrological applications in complex topography. *Hydrology* **2017**, *4*, 53. [CrossRef]
41. Berezowski, T.; Szczeniak, M.; Kardel, I.; Michalowski, R.; Okruszko, T.; Mezghani, A.; Piniewski, M. CPLFD-GDPT5: High-resolution gridded daily precipitation and temperature data set for two largest Polish river basins. *Earth Syst. Sci. Data* **2016**, *8*, 127–139. [CrossRef]
42. Piniewski, M.; Szcześniak, M.; Kardel, I.; Chattopadhyay, S.; Berezowski, T. G2DC-PL+: A gridded 2 km daily climate dataset for the union of the Polish territory and the Vistula and Odra basins. *Earth Syst. Sci. Data* **2021**, *13*, 1273–1288. [CrossRef]
43. McDonald, J.E. On the Ratio of Evaporation to Precipitation1. *Bull. Am. Meteorol. Soc.* **1961**, *42*, 185–189. [CrossRef]
44. Mann, H.B. Nonparametric Tests against Trend. *Econometrica* **1945**, *13*, 245–259. [CrossRef]
45. Kendall, M.G. A New Measure of Rank Correlation. *Biometrika* **1938**, *30*, 81–93. [CrossRef]
46. Theil, H. A rank-invariant method of linear and polynomial regression analysis. *R. Neth. Acad. Sci.* **1950**, *53*, 386–392, 521–525, 1397–1412.
47. Sen, P.K. Estimates of the Regression Coefficient Based on Kendall's Tau. *J. Am. Stat. Assoc.* **1968**, *63*, 1379–1389. [CrossRef]
48. Radziejewski, M.; Kundzewicz, Z.W. Detectability of changes in hydrological records. *Hydrol. Sci. J.* **2004**, *49*, 39–52. [CrossRef]
49. Greene, C.A.; Thirumalai, K.; Kearney, K.A.; Delgado, J.M.; Schwanghart, W.; Wolfenbarger, N.S.; Thyng, K.M.; Gwyther, D.E.; Gardner, A.S.; Blankenship, D.D. The Climate Data Toolbox for MATLAB. *Geochem. Geophys. Geosyst.* **2019**, *20*, 3774–3781. [CrossRef]
50. Kruskal, W.H.; Wallis, W.A. Use of Ranks in One-Criterion Variance Analysis. *J. Am. Stat. Assoc.* **1952**, *47*, 583–621. [CrossRef]
51. Kundzewicz, Z.W.; Robson, A.J. Change detection in hydrological records—A review of the methodology/Revue méthodologique de la détection de changements dans les chroniques hydrologiques. *Hydrol. Sci. J.* **2004**, *49*, 7–19. [CrossRef]
52. Radziejewski, M.; Kundzewicz, Z.W. *Development, Use and Application of the Hydrospect Data Analysis System for the Detection of Changes in Hydrological Time-Series for Use in WCP-Water and National Hydrological Services*; WCASP-65; WMO: Geneva, Switzerland, 2004; pp. 1–44.
53. Kolecka, N. Greening trends and their relationship with agricultural land abandonment across Poland. *Remote Sens. Environ.* **2021**, *257*, 112340. [CrossRef]
54. Dębski, K. *Hydrologia Kontynentalna. Cz. II. Fizyka Wody, Opady Atmosferyczne i Parowanie*; Wydawnictwa Komunikacyjne: Warszawa, Poland, 1959; pp. 1–547.